Journal of Power Sources 258 (2014) 89–97

Contents lists available at ScienceDirect

Journal of Power Sources

journal homepage: www.elsevier.com/locate/jpowsour

# A three-dimensional pore-scale model of the cathode electrode in polymer-electrolyte membrane fuel cell by lattice Boltzmann method

G.R. Molaeimanesh, M.H. Akbari*

*Center for Fuel Cell Research, School of Mechanical Engineering, Shiraz University, Molla-Sadra Ave., Shiraz 71348-51154, Iran*

## HIGHLIGHTS

- A 3-D lattice Boltzmann model of cathode GDL in PEM fuel cell is presented.
- Non-homogeneity and anisotropy of GDL, and electrochemical reaction are included.
- General orientation of GDL carbon fibers, shapes species and current distributions.
- Normally oriented carbon fibers cause larger current variations on catalyst layer.
- Microstructure must be regarded as an important characteristic of any GDL material.

## ARTICLE INFO

*Article history:*
Received 25 December 2013
Received in revised form
31 January 2014
Accepted 6 February 2014
Available online 18 February 2014

*Keywords:*
PEM fuel cell
Lattice Boltzmann method
Three-dimensional model
GDL microstructure
Electrochemical reaction

## ABSTRACT

High power density, low operation temperature, high efficiency and low emissions have granted proton exchange membrane (PEM) fuel cells the most promising future among all types of fuel cells. The porous electrodes of PEM fuel cells have a complicated, non-homogeneous, anisotropic microstructure. Therefore, pore-scale modeling techniques such as lattice Boltzmann method, which can capture non-homogeneous and anisotropic microstructures, have recently gained a great attention. In the present study, a three-dimensional lattice Boltzmann model of a PEM fuel cell cathode electrode is proposed in which electrochemical reaction on the catalyst layer and microstructure of GDL are taken into account. The model enables us to simulate single-phase, multi-species reactive flow in a heterogeneous, anisotropic gas diffusion layer through an active approach. To show the capability of the proposed model, reactive flow in three reconstructed GDLs with different anisotropic characteristics is simulated to investigate the effects of GDL microstructure on species and current density distributions. The results demonstrate that when carbon fibers are more likely oriented normal to the catalyst layer, species density distribution is thicker and more disturbed. Current density also experiences a larger variation on the catalyst layer in such a case.



## 1. Introduction

A sustainable, high quality life is the basic driver for providing a clean, safe, reliable and secure energy supply in the world. Fuel cells and hydrogen systems are important technologies which may contribute positively to the future world energy demand. Among different types of fuel cells, proton exchange membrane (PEM) fuel cells currently hold the most promising prospect. They can be employed in a wide range of applications, ranging from very small portable devices such as mobile phones and laptops, through transport applications like cars, delivery vehicles, buses and ships, to combined heat and power generators in stationary applications in the domestic and industrial sectors [1].

Nevertheless, some barriers such as high cost and operational difficulties hinder PEM fuel cells' wide commercialization, which make fundamental research for their development inevitable. Modeling of reactant gas transport accompanied by electrochemical reactions in the electrodes is of great importance, especially in the cathode where the oxygen reduction reaction is sluggish and inefficient [2]. Numerous numerical models of the cathode electrode with different features can be found in the literature [3]. In most of these models, the gas diffusion layer (GDL) of cathode electrode is considered as a homogeneous and isotropic porous medium, while in reality that is not the case [4]. In this regard, pore-scale modeling techniques which can realistically capture the microstructure of the cathode GDL are extremely attractive.

Some researchers have used more conventional methods, such as the finite volume, to model electrodes of a PEMFC. Harvey et al. [5], for example, used such a method to investigate different approaches to

* Corresponding author. Tel.: +98 917 308 8424; fax: +98 711 647 3511.
*E-mail addresses:* h-akbari@shirazu.ac.ir, hakbari391@yahoo.com (M.H. Akbari).

http://dx.doi.org/10.1016/j.jpowsour.2014.02.027
0378-7753/

**Nomenclature**

| | |
|---|---|
| $a$ | roughness factor |
| $\vec{c}$ | particle velocity (lu ts$^{-1}$) |
| $c_s$ | speed of sound in lattice (lu ts$^{-1}$) |
| $D$ | diffusivity (m$^2$ s$^{-1}$) |
| $D^{LB}$ | lattice Boltzmann diffusivity |
| $Da$ | Damköhler number |
| $F$ | Faraday's constant (A s mol$^{-1}$) |
| $Fo$ | Fourier number |
| $f$ | density distribution function |
| $j$ | current density (A m$^{-2}$) |
| $k$ | rate constant (m s$^{-1}$) |
| $k^{LB}$ | lattice Boltzmann rate constant |
| $l$ | characteristic length scale (m) |
| MW | molar mass (kg kmol$^{-1}$) |
| $P$ | pressure (Pa) |
| $R_u$ | universal gas constant (J mol$^{-1}$ K$^{-1}$) |
| $\vec{r}$ | particle position vector (lu) |
| $r''$ | reaction rate per unit surface area (mol m$^{-2}$ s$^{-1}$) |
| $T$ | temperature (K) |
| $t$ | time (ts) |
| $\vec{u}$ | velocity vector (lu ts$^{-1}$) |
| $\vec{u}'$ | composite velocity vector in Eq. (5) (lu ts$^{-1}$) |
| $w$ | weighting factor |

*Greek symbols*

| | |
|---|---|
| $\alpha$ | transfer coefficient |
| $\eta$ | activation over-potential |
| $\lambda_n$ | Eigen-parameter in Eq. (11) |
| $\mu$ | dynamic viscosity (kg m$^{-1}$ s$^{-1}$) |
| $\nu$ | kinematic viscosity (lu$^2$ ts$^{-1}$) |
| $\rho$ | density (lm lu$^{-3}$ or kg m$^{-3}$) |
| $\rho^*$ | dimensionless density |
| $\tau$ | relaxation time (ts) |

*Subscripts and superscripts*

| | |
|---|---|
| $A$ | type A species |
| $C$ | type C species |
| eq | equilibrium |
| $i$ | direction $i$ of lattice |
| $k$ | species $k$ |
| LB | lattice Boltzmann |
| $n$ | nitrogen |
| $o$ | oxygen |
| ref | reference |
| sr | surface reaction |
| $w$ | water |

modeling the catalyst layer of PEM fuel cells. They compared three catalyst treatments of thin-film model, discrete-catalyst volume model and agglomerate model, and concluded that only the agglomerate model could capture mass transport limitations that occur at high current densities. Sahraoui et al. [6] presented a two-dimensional, finite-volume model of a PEM fuel cell taking into consideration the finite thicknesses of the catalyst layer and membrane. Sun et al. [7] also introduced a two-dimensional model for PEM fuel cell cathode that treated the catalyst layer as agglomerates of polymer electrolyte coated catalyst particles. They showed that the cathode over-potential inside the catalyst layer was non-uniform influenced by the channel-land geometry.

In the past decade, lattice Boltzmann method has emerged as a powerful pore-scale modeling technique applicable in complicated, heterogeneous, anisotropic porous media such as GDLs of PEM fuel cells. Lattice Boltzmann method is superior to other conventional numerical modeling techniques through many aspects such as capability of dealing with complex boundaries of a complicated microstructure, easy parallelizable algorithm development, and facility in modeling multi-phase fluid flow in a porous medium [8].

However, a significant challenge for lattice Boltzmann modeling of the cathode electrode is a proper way to consider electrochemical reaction in the catalyst layer [9]. To the best of the authors' knowledge the electrochemical reaction is taken into account in only a few two-dimensional lattice Boltzmann investigations, such as those presented by Chen et al. [10–12]; moreover, no such three-dimensional modeling, taking into account the electrochemical reaction, was found in the literature. In the present study, a single-phase, three-dimensional model of the cathode electrode of a PEM fuel cell is presented in which the catalyst layer is considered as a thin interface where the electrochemical reaction occurs. The proposed model is implemented to investigate the effects of GDL microstructure on the distributions of species and current density. An advantage of the proposed model over previous lattice Boltzmann models [10–12] is the use of an active approach for species transport. In the preceding investigations [10–12], a passive approach was applied in which the velocity field is only solved for nitrogen that is taken as the solvent. This may lead to lack of accuracy especially when the density of other species is comparable to that of nitrogen which may happen at high over-potentials; in such cases no species can be considered as a solvent [13]. On the other hand, in an active approach the internally coupled velocity fields of all species are solved individually which can lead to more accurate results.

## 2. Numerical method

### 2.1. Framework of lattice Boltzmann method

Lattice Boltzmann method is a powerful numerical modeling technique that has attracted much interest in the past decade. In this method, a fluid is assumed to be composed of virtual fluid particles which move and collide with each other in a lattice structure. These particles are treated by a distribution function rather than by positions and velocity vectors [14]. This kinetic nature of lattice Boltzmann method provides some superior features relative to other numerical methods, such as the linearity of the transport equation (in comparison with nonlinear Navier–Stokes equations), calculation of pressure by an equation of state (in comparison with calculating the pressure by solving Poisson differential equation), etc. [8].

The present numerical model is based on the lattice-Boltzmann method with a single relaxation time collision operator (the so-called BGK model [15]) and the popular D3Q19 lattice scheme. The 3 in D3Q19 refers to the number of lattice dimensions and the 19 denotes the number of possible directions for a particle movement in the lattice as shown in Fig. 1.

The lattice Boltzmann equation is derived from simplification of Boltzmann equation in a lattice [16]. It can be expressed as

$$f_i(\vec{r}+\vec{c}_i\Delta t, t+\Delta t) = f_i(\vec{r},t) + \frac{\Delta t}{\tau}\left[f_i^{eq}(\vec{r},t) - f_i(\vec{r},t)\right] \quad (1)$$

where $f_i$ is the density distribution function in direction $i$, $f_i^{eq}$ is the equilibrium density distribution function, $\vec{r}$ refers to space position, $t$ is time, $\vec{c}_i$[1] is the particle velocity vector in direction $i$, and $\tau$

[1] lu and ts are the unit of length and time in lattice Boltzmann method, respectively.

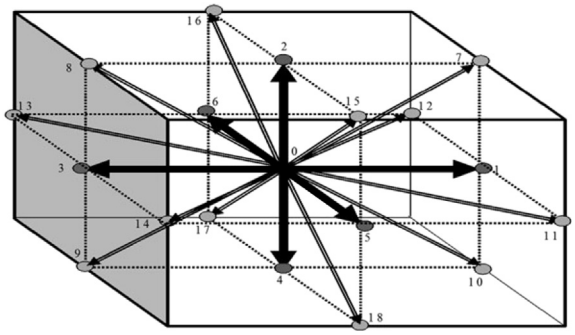

**Fig. 1.** D3Q19 lattice scheme.

is the relaxation time which is related to kinematic viscosity, $\nu$, by $\tau = 3\nu + 1/2$. The equilibrium density distribution function is determined by

$$f_i^{eq} = w_i\rho\left[1 + \frac{\vec{c}_i\cdot\vec{u}}{c_s^2} + \frac{1}{2}\frac{(\vec{c}_i\cdot\vec{u})^2}{c_s^4} - \frac{1}{2}\frac{\vec{u}\cdot\vec{u}}{c_s^2}\right] \quad (2)$$

In this equation, $w_i$ is the weighting factor, $\rho = \sum_i f_i$ is the fluid density, $\vec{u} = \sum_i f_i\vec{c}_i/\sum_i f_i$ is fluid velocity and $c_s$ is the speed of sound in the lattice.

Eq. (1) is solved through collision and streaming processes which are shown for D3Q19 scheme in Eqs. (3) and (4) respectively.

$$f_i(x,y,z,t+\Delta t) = f_i(x,y,z,t)\left[1 - \frac{\Delta t}{\tau}\right] + \frac{\Delta t}{\tau}f_i^{eq}(x,y,z,t) \quad (3)$$

$$f_i(x+\Delta x, y+\Delta y, z+\Delta z, t+\Delta t) = f_i(x,y,z,t+\Delta t) \quad (4)$$

To completely determine density distribution functions, $f_i$ s must be specified at the boundaries. A simple and powerful LBM boundary condition applied to no-slip walls is called bounce back boundary condition. This boundary condition is based on the idea that particles colliding a wall in a direction will bounce back in the opposite direction [17]. In fact, this boundary condition enables LBM to model fluid flow in geometries with complicated microstructure such as pore space of a porous medium. Several versions of this boundary condition have been proposed [13]; however, the mostly used version is half-way method in which the wall is located half-way between two neighboring grids.

### 2.2. Simulation of single-phase multi-component flow

Generally, two passive and active approaches are used for simulating single-phase, multi-component fluid flows. In the passive approach the chemical species whose mass fraction is greater than the others is considered as a solvent while other species are considered as solutes. In this way the velocity field is only solved for the solvent species, followed by the solution of advection–diffusion equation for the other species. Therefore, the velocity field is only dependent on the solvent species. When species concentrations are comparable and no species can be considered as a solvent, this approach may lead to lack of accuracy [13].

On the other hand, in the active approach the internally coupled velocity fields of all species are solved individually; hence, more accurate results can be obtained by the more realistic active approach. To apply this approach in lattice Boltzmann method, multi-phase multi-component models are adopted, and some of their settings are modified to reduce the number of phases to one.

Several multi-phase multi-component lattice Boltzmann models [18–20] have been presented in the literature. In the present study, the Shan and Chen model [19] is selected over other models due to its simplicity and easy implementation. Since the intention here is to model a single-phase reactive flow, the number of phases is reduced to one simply by eliminating the inter-particle forces [13]. Therefore, to implement Shan and Chen model for the single-phase flow consisting of oxygen, nitrogen and water vapor species, streaming and collision processes are solved individually for each species to find $f_i^k$, where the superscript $k$ denotes the $k$th chemical species. However, in collision process instead of $\vec{u}^k$ in Eq. (2), the composite velocity, $\vec{u}'$, must be incorporated to couple the species lattice Boltzmann equations. The composite velocity is defined as

$$\vec{u}' = \frac{\sum_k \frac{1}{\tau^k}\sum_i f_i^k\vec{c}_i}{\sum_k \frac{1}{\tau^k}\rho^k} \quad (5)$$

In the above equation $\rho^k = \sum_i f_i^k$ is the density of species $k$ and $\tau^k$ is the relaxation time of species $k$. This relaxation time is related to the kinematic viscosity of species $k$, $\nu^k$, by the relation $\tau^k = 3\nu^k + 1/2$.

### 2.3. Surface reaction model based on modified bounce back boundary condition

Kamali et al. [21] recently proposed a half-way bounce back boundary condition for simulating surface reaction. Their proposed boundary condition is only applicable to a typical surface reaction $A + B + \ldots \rightarrow C + E + \ldots$ which is first order in $A$; i.e., $r'' = k_{sr}\rho^A$ where $r''$, $k_{sr}$ and $\rho^A$ are the reaction rate per unit area, the rate coefficient and the density of species $A$ at the reactive surface, respectively. They showed that for such a reaction, when a particle of type $A$ hits the wall, fraction $k_{sr}^{LB}$ of its mass is converted into $C$, while the remaining fraction $1 - k_{sr}^{LB}$ of its mass is conserved as $A$, where

$$k_{sr}^{LB} = \left(\frac{6k_{sr}\Delta t}{\Delta x}\right)\Big/\left(1 + \frac{k_{sr}\Delta x}{2D}\right) \quad (6)$$

and $k_{sr}$ is the rate constant of surface reaction, $\Delta t$ and $\Delta x$ are the time and space intervals in direction normal to the surface, and $D$ is the diffusion coefficient of species $A$. Upon calculating $k_{sr}^{LB}$, one can easily modify bounce back boundary condition to simulate a surface reaction. For instance, if a particle of type $A$ moving from left to right hits a vertical wall on its path, its bounced back distribution function will be

$$\begin{aligned} f_3^A &= \left(1 - k_{sr}^{LB}\right)f_1^A \\ f_8^A &= \left(1 - k_{sr}^{LB}\right)f_{10}^A \\ f_9^A &= \left(1 - k_{sr}^{LB}\right)f_7^A \\ f_{13}^A &= \left(1 - k_{sr}^{LB}\right)f_{11}^A \\ f_{14}^A &= \left(1 - k_{sr}^{LB}\right)f_{12}^A \end{aligned} \quad (7)$$

and the bounced back distribution function of a particle of type $C$ will be

$$\begin{aligned} f_3^C &= \frac{MW_C}{MW_A}k_{sr}^{LB}f_1^A + f_1^C \\ f_8^C &= \frac{MW_C}{MW_A}k_{sr}^{LB}f_{10}^A + f_{10}^C \\ f_9^C &= \frac{MW_C}{MW_A}k_{sr}^{LB}f_7^A + f_7^C \\ f_{13}^C &= \frac{MW_C}{MW_A}k_{sr}^{LB}f_{11}^A + f_{11}^C \\ f_{14}^C &= \frac{MW_C}{MW_A}k_{sr}^{LB}f_{12}^A + f_{12}^C \end{aligned} \quad (8)$$

where $MW_A$ and $MW_C$ are the molar masses of $A$ and $C$, respectively. Obviously when the surface reaction is very fast ($k_{sr} \rightarrow \infty$), all the mass of a particle of type $A$ will be consumed, thus $\sum_i f_i^A$ will

become zero. Therefore, considering Eq. (7), $k_{sr}^{LB}$ must become equal to 2 or $\lim_{k_{sr}\to\infty} k_{sr}^{LB} = 2$. Consequently, $\Delta t$ in Eq. (6) must be chosen as

$$\Delta t = \frac{\Delta x^2}{6D} \tag{9}$$

### 2.4. Validation of surface reaction model

Kamali et al. [21] validated their proposed LB model by the analytical solution of a one-dimensional reaction-diffusion problem which is only valid for $Fo << 1$ where Fourier number is $Fo = Dt/l^2$. Since this condition is not necessarily valid in a PEM fuel cell electrode, we have validated the model against the analytical solution of another one-dimensional reaction-diffusion problem which is valid for all $Fo$ values. The problem is a one-dimensional diffusion in an infinite channel with two symmetric reactive surfaces (width $= 2l$) as shown in Fig. 2. It is obvious that at the symmetry line ($x = 0$), the density gradient is zero. Thus, the partial differential equation and the initial and boundary conditions that describe the problem are

$$\begin{aligned} &\frac{\partial \rho_A}{\partial t} = D\frac{\partial^2 \rho_A}{\partial x^2} \\ &\rho_A(x, t = 0) = 1 \\ &\left.\frac{\partial \rho_A}{\partial t}\right|_{x=0} = 0 \\ &\left.\frac{\partial \rho_A}{\partial t}\right|_{x=l} = -k_{sr}\rho_A(x = l) \end{aligned} \tag{10}$$

where $\rho_A$ is the density of species $A$. After converting Eq. (10) to a non-dimensional form and by the aid of separation of variables, the solution will be obtained as

$$\rho_A^*(x,t) = \sum_{n=1}^{\infty} \frac{4\sin(\lambda_n)}{2\lambda_n + \sin(2\lambda_n)} e^{-\lambda_n^2 Fo} \cos\left(\lambda_n \frac{x}{l}\right) \tag{11}$$

In this equation $\rho_A^*$ is the non-dimensional density of species $A$, and $\lambda_n$ are the eigen-parameters which are the roots of equation $\lambda_n \tan(\lambda_n) = Da$ (given in Ref. [22]), where Damköhler number is defined as $Da = lk_s/D$. The analytical solution is computed for the first six terms for several $Da$ and $Fo$ and are compared with the corresponding lattice Boltzmann method results in Fig. 3. It is clearly observed in this figure that the lattice Boltzmann method results are in a very good agreement with the analytical solution for all values of $Da$ and $Fo$ numbers.

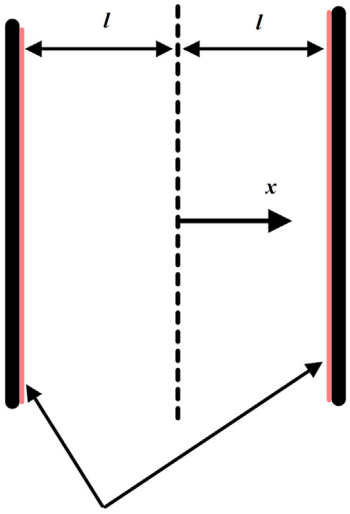


**Fig. 2.** Scheme of the problem used for the validation of the modified bounce back boundary condition.

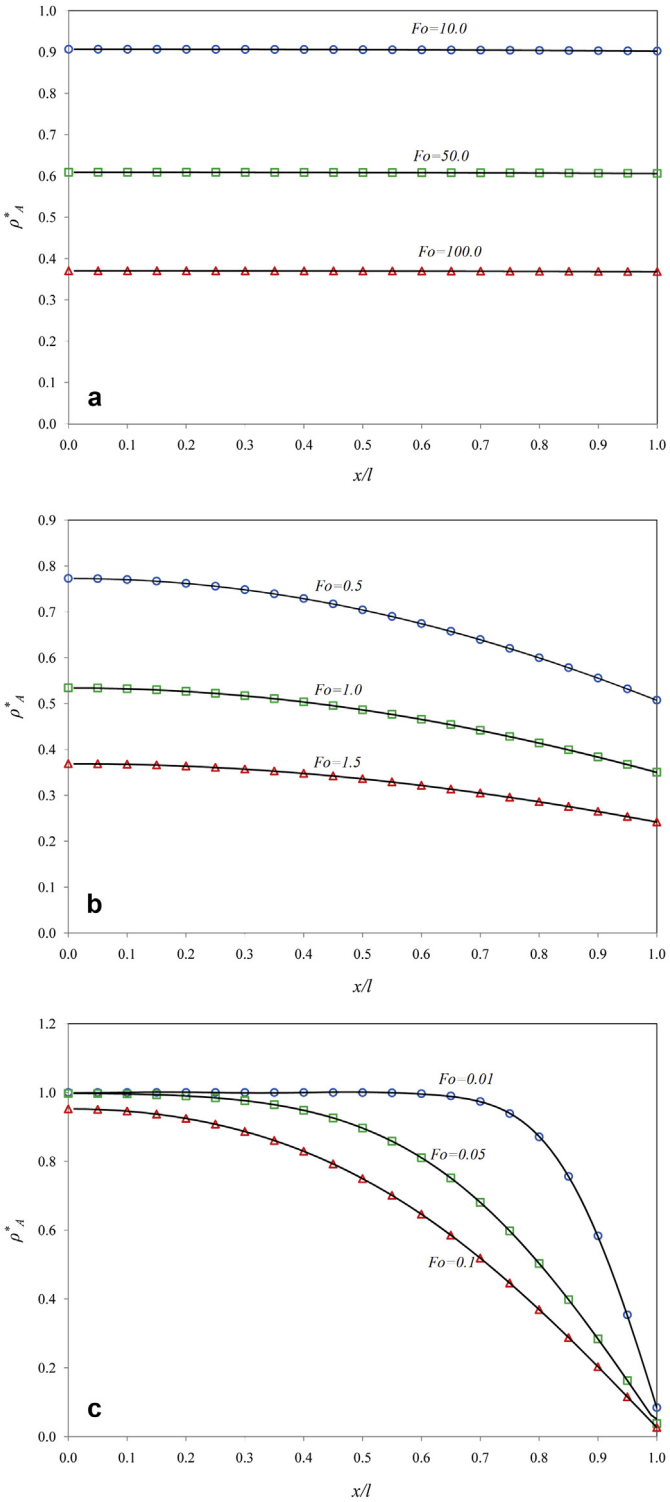


**Fig. 3.** Validation of the modified bounce back boundary condition by analytical solution of a diffusion problem in an infinite slab with reactive surfaces at various Fourier and Damköhler numbers: (a) $Da = 0.01$, (b) $Da = 1$, (c) $Da = 100$; symbols: lattice Boltzmann simulation, solid lines: analytical solution.

### 2.5. Electrochemical reaction

The electrochemical reaction at the PEM fuel cell cathode electrode is the oxygen reduction reaction as follows

$$O_2 + 4H^+ + 4\bar{e} \leftrightarrow 2H_2O \tag{12}$$

The rate of this reaction per unit area, $r''$, is directly proportional to the current density, $j$, through $r'' = j/4F$ where $F$ is the Faraday's constant. On the other hand, current density is a function of oxygen concentration and activation over-potential through Butler–Volmer equation [2]. Therefore, after some manipulation the rate equation for the electrochemical reaction on the catalyst layer, which is assumed to be a thin interface, can be expressed as

$$r'' = \left\{ \frac{a}{4F} \left( \frac{j^{\text{ref}}}{\rho^{o,\text{ref}}} \right) \left[ \exp\left( \frac{\alpha_f F \eta}{R_u T} \right) - \exp\left( -\frac{\alpha_r F \eta}{R_u T} \right) \right] \right\} \rho^o \tag{13}$$

where $a$ is the roughness factor of catalyst layer, $j^{\text{ref}}$ is the reference current density, $\rho^{o,\text{ref}}$ is the reference oxygen density, $\alpha_f$ is the transfer coefficient for the forward reaction, $\alpha_r$ is the transfer coefficient for the reverse reaction, $\eta$ is the activation over-potential and $\rho^o$ is the oxygen density on the catalyst layer. Eq. (13) can be expressed as $r'' = k_{\text{sr}} \rho^o$ where $k_{\text{sr}}$, the rate constant of the electrochemical reaction on the catalyst layer, is equal to

$$k_{\text{sr}} = \frac{a}{4F} \left( \frac{j^{\text{ref}}}{\rho^{o,\text{ref}}} \right) \left[ \exp\left( \frac{\alpha_f F \eta}{R_u T} \right) - \exp\left( -\frac{\alpha_r F \eta}{R_u T} \right) \right] \tag{14}$$

Upon calculation of $k_{\text{sr}}$, $k_{\text{sr}}^{\text{LB}}$ can be calculated for the electrochemical reaction on the catalyst layer through Eq. (6) and then, by applying the proposed modified bounce back boundary condition, the entire cathode electrode can be simulated through an active approach.

## 3. Three-dimensional reconstruction of GDL microstructure

In the early efforts of lattice Boltzmann simulation of fluid flow in pore spaces of a GDL, very simplified microstructures were used [23,24]. However, with today's enhancement of electron microscopy methods, more realistic delineations of GDL microstructure can be provided by different three-dimensional reconstruction methods. Generally, the implemented methods for three-dimensional reconstruction of a GDL can be classified into two categories: imaging combination and stochastic generation. The former captures sequential images of a GDL scanned by X-ray or scanning laser microscopy, and then integrates these images to reconstruct the three-dimensional GDL microstructure. The later reconstructs the porous medium microstructure based on the statistical information of the GDL microstructure. The low cost and easy implementation make the stochastic generation method a more convenient choice for us than the imaging combination method [25]. The GDL microstructure in most of three-dimensional lattice Boltzmann simulations were reconstructed by stochastic generation methods [26–33]. In the present study, the stochastic generation method proposed by Schladitz et al. [34] is adopted to reconstruct three different carbon paper GDLs which have also been adopted in other lattice Boltzmann simulations [26–31]. The reconstruction method is based on the following assumptions: (a) carbon fibers in GDLs are cylinders having a fixed and uniform radius; (b) fibers are straight and infinitely long; (c) fibers are allowed to overlap. The reconstruction method is started by stochastic generation of a line. Consequently, the nodes of the lattice whose distances from the line are less than or equal to the fiber radius are selected as solid parts. This process is repeated until the required porosity is achieved.

The stochastically generated lines are isotropic in the material plane (the plane of carbon paper) and are anisotropic normal to the material plane. The degree of this anisotropy is recognized by a factor named anisotropy parameter, $\beta$, which is $0 < \beta < \infty$ [34]. If $0 < \beta < 1$, the reconstructed carbon fibers are more probably oriented normal to the material plane, and if $\beta > 1$, the reconstructed carbon fibers are most likely oriented parallel to the material plane; if $\beta = 1$, the reconstructed carbon fibers take a completely isotropic distribution. For practical GDLs the anisotropy parameter is a large number which indicates that most of carbon fibers are parallel to the material plane. Schulz et al. [25] have reported the anisotropy parameter, fiber diameter and porosity for Toray090 carbon paper as 10000, 7 μm and 78%, respectively. In the present study, the Toray090 is reconstructed in a lattice with $101 \times 101 \times 101$ nodes using the reported data of Schulz et al. [25] as shown in Fig. 4(a). In addition, as shown in Fig. 4(b) and (c), two other GDLs are reconstructed with the same lattice size, fiber diameter and porosity, but with different anisotropy parameters of 1 and 0.01.

## 4. Computational domain and boundary conditions

The computational domain consists of a portion of GDL, catalyst layer and land as shown in Fig. 5. As mentioned previously, the catalyst layer is simply treated as a thin interface on the bottom surface of the computational domain on which electrochemical reaction occurs. Two opposite lateral sides of computational domain are considered as the inlet (plane $x = 0$) and outlet (plane $x = 100$ μm), while the other two lateral sides (planes $y = 0$ and $y = 100$ μm) are assumed as symmetry planes.

The inlet flow is taken as dry air at 1.5 atm pressure with oxygen to nitrogen molar ratio of 21/79 which reacts on the catalyst layer and produces water vapor. A constant pressure boundary condition is applied on the outlet such that a constant pressure differential of 0.001 atm exists between the inlet and outlet. To implement the constant pressure boundary conditions, the Zou and He method [35] is utilized. Since only the outlet total pressure is known and the outlet partial pressure of each species is unknown, these partial pressures are determined by assuming that the mole fraction of each species at the outlet is equal to that at the preceding nodes; this is a reasonable assumption since species fraction will not change much through a lattice unit (1 μm). Upon determining outlet partial pressure of each species, constant pressure boundary condition of Zou and He [35] is applied for each species. The no-slip boundary condition is considered on the surfaces of all non-reactive solid parts. All species are considered as ideal gases with different kinematic viscosities.

Simulations are performed on a desktop computer using a parallel FORTRAN code developed in house, based on the proposed model. The value of simulation parameters are given in Table 1.

## 5. Preliminary results and discussion

The purpose of this article is to present the details of the proposed three-dimensional model for the cathode electrode of a PEM fuel cell. Therefore, only some preliminary results are presented here to demonstrate the capabilities of the model. Further simulations will be performed to investigate more thoroughly the effects of realistic microstructure of GDLs on a PEM fuel cell performance. Such simulations will require more sophisticated computational facilities that are not currently available to the authors.

Presented in the following are the simulation results for the GDLs described in Section 3 and illustrated in Fig. 4(a)–(c).

Oxygen mole fraction distributions in the three reconstructed GDLs are shown in Fig. 6. Cross sections of carbon fibers are indicated in these figures in heavy black color. Obviously, for

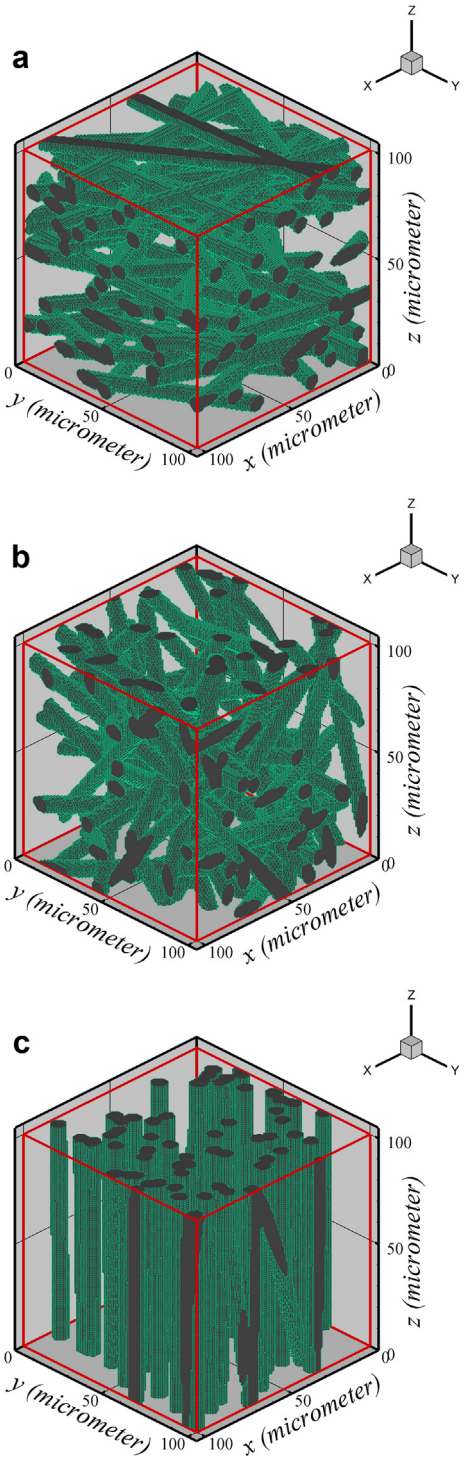


**Fig. 4.** Reconstructed GDLs with different anisotropy parameters: (a) $\beta = 10000$, (b) $\beta = 1$, (c) $\beta = 0.01$.

horizontally oriented carbon fibers the cross section looks more circular (Fig. 6(a)) in a lateral plane, while for more vertically oriented fibers the cross section looks similar to an elongated ellipse (Fig. 6(c)). It is also reminded that the larger the anisotropy parameter, the higher probability of horizontal orientation of the carbon fibers.

It is clear in Fig. 6 that mole fraction of oxygen decreases while it is penetrating toward the catalyst layer. Oxygen consumption on the catalyst layer also causes its mole fraction to decrease along the

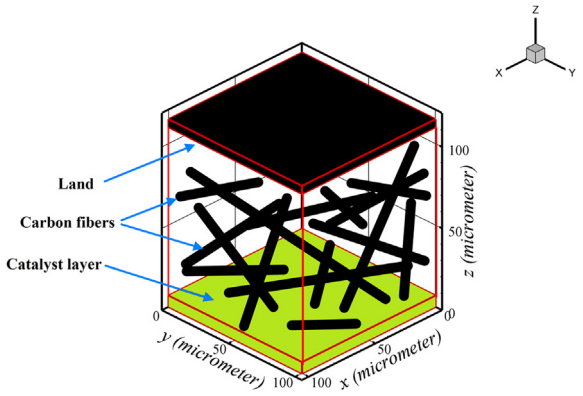


**Fig. 5.** Computational domain consisting of a portion of GDL, catalyst layer and land.

bulk flow direction ($x$-axis). However, this trend is reversed near the outlet because of the effects of the GDL pore microstructure.

A comparison among Fig. 6(a)–(c) shows that GDL microstructure greatly influences species distribution in the cathode. More specifically, it is observed that when carbon fibers are mostly oriented normal to the catalyst layer then oxygen density boundary layer will be thicker. In other words, in this situation the boundary layer is disturbed more strongly by the fibers, hence a thicker boundary layer.

Similarly, water vapor mole fraction distributions in the three reconstructed GDLs are presented in Fig. 7. Again, due to its production by electrochemical reaction on the catalyst layer, water vapor mole fraction increases both normal to the catalyst layer and in the bulk flow direction. In fact, there can be observed a correspondence between the distributions of oxygen and water vapor species shown in Figs. 6 and 7, since water production rate is directly related to oxygen concentration.

Fig. 7(a)–(c) illustrates how greatly GDL microstructure can affect species distribution. Similar to oxygen, water vapor density boundary layer is more disturbed when carbon fibers are mostly oriented normal to the catalyst layer in a GDL (with lower anisotropy parameter), hence a thicker boundary layer. Disturbance of boundary layer of water vapor density may be regarded as a desirable event, since it can lower the water vapor density near the catalyst layer which can mitigate flooding of the GDL. Therefore, the effects of GDL pore microstructure on the form of water produced must be investigated more thoroughly to help enhance PEMFC water management.

**Table 1**
Values of simulation parameters.

| Parameter | Value |
|---|---|
| Operating temperature, $T$ | 353 K |
| Operating pressure, $P$ | 1.5 atm |
| Pressure differential between the inlet and the outlet | 0.001 atm |
| Water vapor mole fraction in the inlet air | 0.0 |
| Oxygen mole fraction in the inlet air | 0.21 |
| Nitrogen mole fraction in the inlet air | 0.79 |
| Dynamic viscosity of oxygen, $\mu^o$ | $2.34 \times 10^{-5}$ kg m$^{-1}$ s$^{-1}$ [36] |
| Dynamic viscosity of nitrogen, $\mu^n$ | $2.01 \times 10^{-5}$ kg m$^{-1}$ s$^{-1}$ [36] |
| Dynamic viscosity of water vapor, $\mu^w$ | $1.20 \times 10^{-5}$ kg m$^{-1}$ s$^{-1}$ [36] |
| Oxygen diffusivity in the mixture ($Do$) | $1.891 \times 10^{-5}$ m$^2$ s$^{-1}$ [37] |
| Reference oxygen concentration ($\rho^{o,\mathrm{ref}}$) | 10.875 mol m$^{-3}$ [37] |
| Roughness factor ($a$) | 2000 [38] |
| Reference current density ($j^{\mathrm{ref}}$) | $1.3874 \times 10^{-2}$ A m$^{-2}$ [39] |
| Transfer coefficient for forward oxygen reduction ($\alpha_f$) | 0.5 [40] |
| Transfer coefficient for reverse oxygen reduction ($\alpha_r$) | 1 [40] |

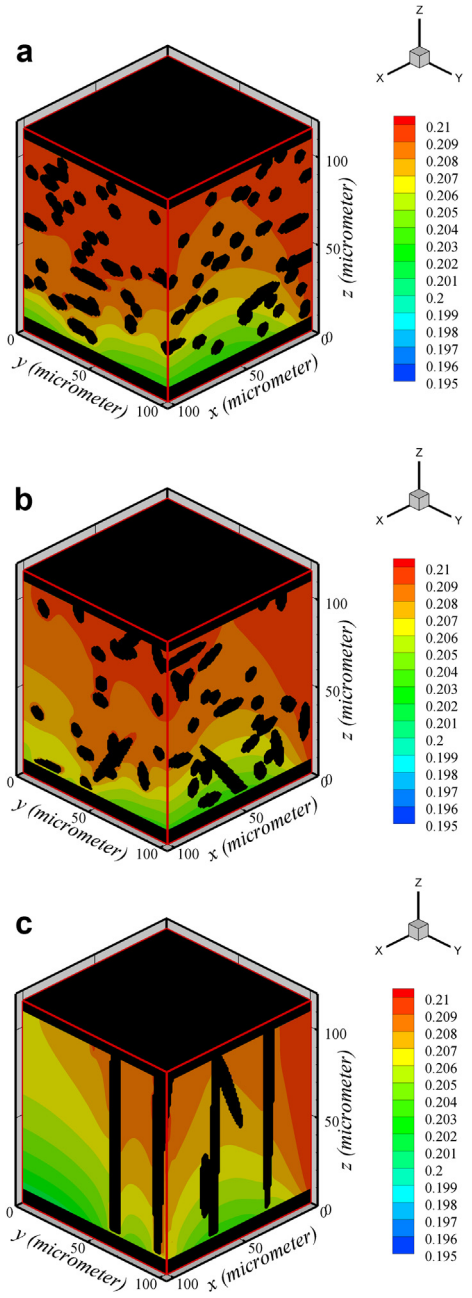


**Fig. 6.** Oxygen mole fraction distribution in the three reconstructed GDLs: (a) $\beta = 10000$, (b) $\beta = 1$, (c) $\beta = 0.01$.

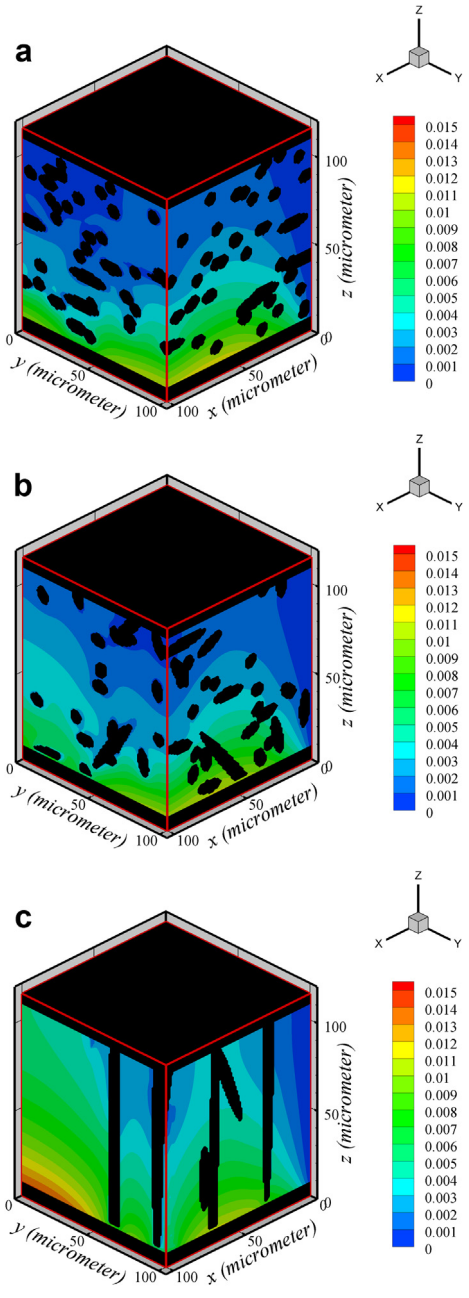


**Fig. 7.** Water vapor mole fraction distribution in the three reconstructed GDLs: (a) $\beta = 10000$, (b) $\beta = 1$, (c) $\beta = 0.01$.

Shown in Fig. 8 are current density distributions on the catalyst layer for the three simulated cases. The current densities shown here correspond to the "surface" of the catalyst layer. As mentioned before, the catalyst layer in our simulations is considered as an interface between the GDL and membrane, which acts as a charge conductor itself. The current density decreases in the bulk flow direction ($x$-axis) due to oxygen consumption on the catalyst layer. However, locations of the minimum current density are different in the three cases, which indicate the influence of GDL microstructure on current density distribution.

Although the variations in current density may seem small, but one must realize that the simulation scale is also small, i.e., current density variation may be much larger for practical sizes of the catalyst layer.

An examination of Fig. 8(a)–(c) reveals that when carbon fibers are mostly oriented normal to catalyst layer (i.e., smaller anisotropy parameter) a larger variation in current density is observed. This may be the result of thicker oxygen density boundary layer in such a case. The larger variation observed in Fig. 8(c) matches with the lowest overall current density among the cases when carbon fibers are mostly oriented normal to catalyst layer. Apparently, this is caused by more severe limitation of oxygen transport to the surface of the catalyst layer due to the mostly vertical orientation of the GDL fibers.

A comparison of Fig. 6(a)–(c) shows that the oxygen mole fraction near the catalyst layer around point $x = 100$ μm, $y = 100$ μm in Fig. 6(a) is the lowest among the cases; accordingly, current density at this corner in Fig. 8(a) is also the lowest in Fig. 8(a)–(c).

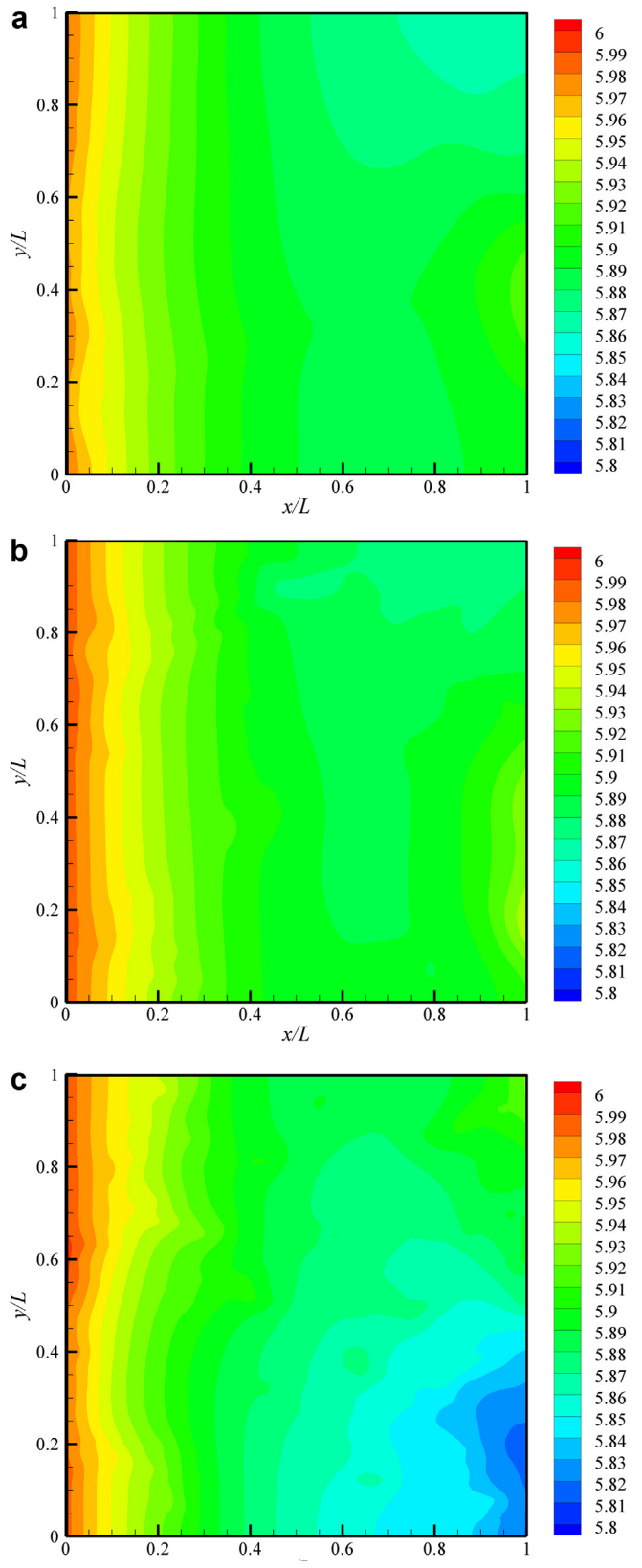


**Fig. 8.** Current density distribution on the catalyst layer for the three reconstructed GDLs simulated: (a) $\beta = 10000$, (b) $\beta = 1$, (c) $\beta = 0.01$.

Considering the results given in Figs. 7 and 8, it is observed that when the orientation of carbon fibers is dominated in the horizontal direction (parallel to the catalyst layer), a more uniform current density distribution is obtained (desirable), while water vapor density is also greater near the catalyst layer in this case (undesirable). It may suggest that for practical purposes, a GDL microstructure must be prevented from being dominated by carbon fibers oriented in either horizontal or vertical directions relative to the catalyst layer.

Practical GDLs are of different types (such as paper, cloth and felt) and are produced by different companies using different techniques; hence, they certainly hold different microstructures. Moreover, GDL microstructure can be altered during stack assembly due to compression of the cells. On the other hand, the results from the present and similar studies clearly show that GDL microstructure has definite effects on species and current density distributions. Hence, the microstructure must be regarded as an important characteristic of any GDL material, and further research on its effects must be pursued.

## 6. Conclusions

In the present study, a three-dimensional pore-scale model based on lattice Boltzmann method is proposed for the cathode electrode of a PEM fuel cell, taking into account the electrochemical reaction on the catalyst layer and microstructure of the GDL. The model enables us to simulate single-phase, multi-species reactive flow in a heterogeneous, anisotropic GDL through an active approach. Reactive flow in three reconstructed GDLs with different anisotropy parameters is simulated to investigate the effects of GDL microstructure on species and current density distributions. The results demonstrate that when carbon fibers are mostly oriented normal to the catalyst layer, oxygen and water vapor density boundary layers will be thicker and more disturbed. Current density variation on the catalyst layer will be also more profound in such a case.

Results of the present study display the important role of numerical methods capable of taking into account the non-homogeneity and anisotropy of GDL microstructure, such as lattice Boltzmann method. These models allow one to hold a more clear understanding of fundamental phenomena that occur in a PEM fuel cell electrode.

## References

[1] J. Larminie, A. Dicks, Fuel Cell Systems Explained, second ed., John Wiley & Sons, Chichester, 2003.
[2] Y. Wang, K.S. Chen, J. Mishler, S.C. Cho, X.C. Adroher, Appl. Energy 88 (2011) 981–1007.
[3] M.A. Khan, B. Sundén, J. Yuan, J. Power Sources 196 (2011) 7899–7916.
[4] H. Ostadi, P. Rama, Y. Liu, R. Chen, X. Zhang, K. Jiang, Microelectron. Eng. 87 (2010) 1640–1642.
[5] D. Harvey, J.G. Pharoah, K. Karan, J. Power Sources 179 (2008) 209–219.
[6] M. Sahraoui, C. Kharrat, K. Halouani, Int. J. Hydrogen Energy 34 (2009) 3091–3103.
[7] W. Sun, B.A. Peppley, K. Karana, Electrochim. Acta 50 (2005) 3359–3374.
[8] S. Chen, G.D. Doolen, Annu. Rev. Fluid Mech. 30 (1998) 329–364.
[9] A.A. Shah, K.H. Luo, T.R. Ralph, F.C. Walsh, Electrochim. Acta 56 (2011) 3731–3757.
[10] L. Chen, H.B. Luan, Y.L. He, W.Q. Tao, Int. J. Therm. Sci. 5 (2012) 132–144.
[11] L. Chen, H. Luan, Y. Feng, C. Song, Y.L. He, W.Q. Tao, Int. J. Heat Mass Transfer 55 (2012) 3834–3848.
[12] L. Chen, Y.L. Feng, C.X. Song, L. Chen, Y.L. He, W.Q. Tao, Int. J. Heat Mass Transfer 63 (2013) 268–283.
[13] M.C. Sukop, D.T. Thorne, Lattice Boltzmann Modeling, An Introduction for Geoscientists and Engineers, first ed., Springer, Heidelberg, 2007.
[14] A. Satoh, Introduction to Practice of Molecular Simulation, first ed., Elsevier Inc., Amsterdam, 2011.
[15] P.L. Bhatnagar, E.P. Gross, M. Krook, Phys. Rev. 94 (1954) 511–525.
[16] A.A. Mohamad, Lattice Boltzmann Method, Fundamentals and Engineering Applications with Computer Codes, Springer, 2011.

[17] S. Succi, The Lattice Boltzmann Equation for Fluid Dynamics and Beyond Numerical Mathematics and Scientific Computation, first ed., Clarendon Press, Oxford, 2001.
[18] A.K. Gunstensen, D.H. Rothman, S. Zaleski, G. Zanetti, Phys. Rev. A 43 (1991) 4320–4327.
[19] X. Shan, H. Chen, Phys. Rev. E 47 (1993) 1815–1820.
[20] M.R. Swift, W.R. Osborn, J.M. Yeomans, Phys. Rev. Lett. 75 (1995) 830–833.
[21] M.R. Kamali, S. Sundaresan, H.E.A. Van den Akker, J.J.J. Gillissen, Chem. Eng. J. 207–208 (2012) 587–595.
[22] J.H. VanSant, Conduction Heat Transfer Solutions, Lawrence Livermore National Laboratory, California, 1983.
[23] J. Park, M. Matsubara, X. Li, J. Power Sources 173 (2007) 404–414.
[24] Y. Tabe, Y. Lee, T. Chikahisa, M. Kozakai, J. Power Sources 193 (2009) 24–31.
[25] V.P. Schulz, J. Becker, A. Wiegmann, P.P. Mukherjee, C.Y. Wang, J. Electrochem. Soc. 154 (2007) B419–B426.
[26] J. Park, X. Li, J. Power Sources 178 (2008) 248–257.
[27] L. Hao, P. Cheng, J. Power Sources 186 (2009) 104–114.
[28] L. Hao, P. Cheng, J. Power Sources 190 (2009) 435–446.
[29] L. Hao, P. Cheng, J. Power Sources 195 (2010) 3870–3881.
[30] L. Hao, P. Cheng, Int. J. Heat Mass Transfer 55 (2012) 133–139.
[31] P.P. Mukherjee, C.Y. Wang, Q. Kang, Electrochim. Acta 54 (2009) 6861–6875.
[32] D. Froning, J. Brinkmann, U. Reimer, V. Schmidt, W. Lehnert, D. Stolten, Electrochim. Acta 110 (2013) 325–334.
[33] N. Zamel, J. Becker, A. Wiegmann, J. Power Sources 207 (2012) 70–80.
[34] K. Schladitz, S. Peters, D. Reinel-Bitzer, A. Wiegmann, J. Ohser, Comput. Mater. Sci. 38 (2006) 56–66.
[35] Q. Zou, X. He, Phys. Fluids 9 (1997) 1591–1598.
[36] F.P. Incropera, D.P. DeWitt, T.L. Bergman, A.S. Lavine, Fundamentals of Heat and Mass Transfer, sixth ed., John Wiley and Sons, New Jersey, 2007.
[37] M.M. Mench, Fuel Cell Engines, first ed., John Wiley & Sons, New Jersey, 2008.
[38] X. Li, Principles of Fuel Cells, first ed., Taylor and Francis Group, New York, 2006.
[39] A. Parthasarathy, S. Srinivasan, A.J. Appleby, C.R. Martin, J. Electrochem. Soc. 139 (1992) 2530–2537.
[40] T. Berning, D.M. Lu, N. Djilali, J. Power Sources 106 (2002) 284–294.